

On the potential value of Ca II K spectroheliogram time-series for solar activity and irradiance studies

I. Ermolli¹, S. K. Solanki², A. G. Tlatov³, N. A. Krivova², R. K. Ulrich⁴ and J. Singh⁵

¹ INAF - Osservatorio astronomico di Roma, Via Frascati 33, 00040 Monte Porzio Catone, Italy

² Max-Planck-Institut für Sonnensystemforschung, Max-Planck-Strasse 2, 37191 Katlenburg-Lindau, Germany

³ Kislovodsk Solar Station, Pulkovo Observatory, Pulkovskoe Ch. 65-1, 196140 Saint Petersburg, Russia

⁴ Division of Astronomy and Astrophysics, University of California, 8371 Mathematical Science Building, Los Angeles, CA 90095-1562, USA

⁵ Indian Institute of Astrophysics, 2nd Block, Koramangala, 560034 Bangalore, India

ABSTRACT

Context. Various observatories around the globe started regular full-disk imaging of the solar atmosphere in the Ca II K line since the early decades of the 20th century. The archives made by these observations have the potential of providing far more detailed information on solar magnetism than just the sunspot number and area records to which most studies of solar activity and irradiance changes are restricted.

Aims. We evaluate the image contents of three Ca II K spectroheliogram time-series, specifically those obtained by the digitization of the Arcetri, Kodaikanal, and Mt Wilson photographic archives, in order to estimate their value for studies focusing on time-scales longer than the solar cycle.

Methods. We describe the main problems afflicting these data and analyze their quality by expressing the image contents through several quantities. We compare the results obtained with those for similar present-day observations taken with the Meudon spectroheliograph and with the Rome-PSPT.

Results. We show that historic data suffer from stronger geometrical distortions and photometric uncertainties than similar present-day observations. The latter uncertainties mostly originate from the photographic calibration of the original data and from stray-light effects. We also show that the image contents of the three analyzed series vary in time. These variations are probably due to instrument changes and aging of the spectrographs used, as well as changes of the observing programs. Our results imply that the main challenge for the analysis of historic data is their accurate photometric calibration. This problem must be solved before they can provide reliable information about solar magnetism and activity over the last century. Moreover, inter-calibration of results obtained from independent time-series is required to reliably trace changes of solar properties with time from the analysis of such data.

Key words. Sun: activity - Sun: chromosphere - Sun: faculae, plagues - Methods: data analysis

1. Introduction

A wide variety of solar research, ranging from the investigation of global solar activity and variability to the study of large scale patterns of proper motions, is based upon the analysis of regular full-disk observations of the Sun. Only during the last solar cycle have such observations been carried out by space-based telescopes and by the new generation of ground-based instruments, e.g. by SoHO/MDI (Scherrer et al. 1995), PSPT (Coulter & Kuhn 1994; Ermolli et al. 1998), CFDT2-SFO (Chapman et al. 2004), and SOLIS (Keller, Harvey & The Solis Team 2003). These observations are thus of limited usefulness for focussing on time-scales longer than the activity cycle. For such studies regular full-disk observations of the solar atmosphere starting at the beginning of the 20th century at several observatories are of particular interest (for a list of synoptic programs carried out before 1950 see Mouradian & Garcia 2007). These historic observations were made in white light and in various spectral bands,

often in the Ca II K and H α resonance lines, mostly using spectroheliographs.

Among the historic series, those including Ca II K observations have the largest potential of providing information about solar magnetism. In fact, Ca II K emission can be used as a good proxy of the line-of-sight magnetic flux density (Skumanich, Smythe, & Frazier 1975; Schrijver et al. 1989; Ortiz & Rast 2005). Note that in standard notation K_3 , $K_{2V,2R}$, and $K_{1V,1R}$ mark the core, the reversal, and the secondary minimum of the doubly-reversed profile of the Ca II K line, in the violet (V) and the red (R) wings of the line, respectively. All these line features occur within a spectral range less than 1 Å wide.

In principle, historic Ca II K observations constitute an extremely valuable resource for many research topics. However, to date analysis of the Ca II K spectroheliogram time-series was restricted for two reasons: 1) lack of data in digital format; 2) shortcomings and defects that beset historic data. The first restriction should be overcome soon by the results of new projects devoted to the digitization of some of the major photographic archives. For instance, Arcetri, Kodaikanal and Mt Wilson Ca II K historic observations have already been digitized (Ulrich et al. 2004;

Makarov et al. 2004; Marchei et al. 2006), and other similar series are now being processed as well. Defects in and decay of spectroheliogram photographic plates, missing photographic calibration and undocumented changes of the used instrumentation, however, lead to various artifacts in and problems with the historic data (Zharkova et al. 2003; Fuller et al. 2005; Ermolli et al. 2007), which are avoided in the full-disk images taken by the most recent synoptic observing programs.

Here we intercompare and discuss three time-series of images obtained by the digitization of Ca II K historic spectroheliograms. We describe the main problems affecting these data (Sect. 2) and analyze their quality (Sect. 3). In particular, we measure the image contents of these data and compare the results with those obtained for similar present-day observations. The objective of this study is twofold. First of all, it should help to estimate the value of Ca II K historic observations for studies of solar activity, magnetism and irradiance on time-scales longer than the activity cycle (Sects. 4, 5). Secondly, it should raise our understanding of the characteristics that an appropriate image processing technique must have for uniform and accurate application to such data. We see this study as the first step towards a systematic exploitation of this valuable resource.

2. Data, definitions and pre-processing

2.1. Data description

The current analysis concentrates mainly on images obtained from the digitization of Ca II K spectroheliograms stored in the photographic archives of the Arcetri, Kodaikanal and Mt Wilson Observatories (henceforth referred to as historic data). In addition, we have also analyzed samples of Ca II K images obtained by two current synoptic programs, namely those carried out with the Meudon spectroheliograph and with the Rome-PSPT telescope (henceforth referred to as modern data).

Historic data - The first set of spectroheliograms analyzed here was recorded at the G. B. Donati tower of the INAF Arcetri Astrophysical Observatory in Florence from 1931 to 1974 (*Ar*, hereafter). The spectroheliograph used for these observations (Godoli & Righini 1950; Gasperini, Mazzoni, & Righini 2004) had a grating of 600 lines/mm and a ruled area of 100×110 mm, with a dispersion of $0.33 \text{ mm}/\text{\AA}$ at 3934 \AA . The size of the solar disk on most plates is ≈ 6.5 cm; the image scale is thus about $0.033 \text{ mm}/''$. The spectral window for these observations was 0.3 \AA centered in the line core. The instrumentation used to acquire these observations is no longer available.

It is worth noting that several instrumental changes occurred during the over forty years that the spectroheliograph was utilized. These include the use of additional lenses and changes of the slits positions, which improved the image definition and monochromaticity, and decreased the stray-light level. The problem of discontinuities marked by instrumental changes is common to most, if not all, the existing long time-series of synoptic observations. The effects of instrumental changes upon the quality of the data analyzed in this study are presented in Sect. 3.

The digitization of the Arcetri archive was performed by the CVS project at the Rome Astronomical Observatory (Centrone et al. 2005; Giorgi et al. 2005; Marchei et al. 2006). The work was carried out with a commercial scan-

ner, used with the setting 1200×1200 dpi and 16 bit gray-scale significant data. From these data, which are saved in the TIFF format, 2040×2720 16 bit pixel FITS images for each solar observation were produced. Information about the plate acquisition noted in the observation log-books was included in the FITS headers. The diameter of the solar disk in these images is about 1550 pixels; the pixel scale due to the digitization is thus $\approx 1.2''/\text{pixel}$. The digital archive of Ca II K Arcetri observations contains 5976 spectroheliograms obtained on 5042 observing days. The data analyzed here are the reduced-size ($2 \times$ binned) FITS format images available through the CVS archive¹. We analyzed 4052 images obtained on 3927 observing days.

The second set of spectroheliograms is the one recorded at the Kodaikanal Observatory of the Indian Institute of Astrophysics in Bangalore from 1907 to 1999 (*Ko*, hereafter). The spectrograph used for these observations (Evershed 1911; Bappu 1967) is a two prism instrument, with a dispersion of $0.14 \text{ mm}/\text{\AA}$ near 3930 \AA . The $70 \mu\text{m}$ exit slit of the instrument corresponds to a 0.5 \AA bandpass, which includes K_{232} . The size of the solar disk on most plates is ≈ 6 cm; the image scale is thus about $0.031 \text{ mm}/''$. The instrument used to acquire these observations is still available.

The digitization of the Kodaikanal Ca II K archive (Makarov et al. 2004) was performed using a commercial scanner, used with the setting 1200×1200 dpi and 8 bit gray-scale significant data. The original observations were stored as $\approx 1800 \times 1800$ 8 bit gray-scale JPEG images. The solar disk in the digitized images has a diameter of about 1420 pixels; the pixel scale due to the digitization is thus $1.3''/\text{pixel}$. The digital archive of Kodaikanal Ca II K observations contains 26640 spectroheliograms obtained on 26620 observing days. We analyzed here 19522 images obtained on 19172 observing days.

The third set of spectroheliograms we analyzed is the one taken at the Mt Wilson Observatory from 1915 to 1985 (*MW*, hereafter). The spectroheliograph used at the beginning of these observations (Ellerman 1919) had a grating with 590 lines/mm and a ruled area of 61.5×79 mm. After the first decade of observation this grating was changed, and the ruled area was increased to 103×107 mm. The $80 \mu\text{m}$ exit slit admitted the passage of a band of about 0.2 \AA centered on the Ca II K line core. The size of the solar disk on most plates is ≈ 5 cm; the image scale is thus about $0.026 \text{ mm}/''$.

The Mt Wilson observations were digitized in the framework of a project carried out at UCLA Division of Astronomy (Ulrich et al. 2004; Lefebvre et al. 2005). The work was performed with a commercial scanner, used with the setting 1200×1200 dpi and 16 bit gray-scale significant data. From these data, $\approx 2600 \times 2600$ pixels 16 bit TIFF images were singled out, in which intensity values are stored as positive integers. The solar disk in these images has a diameter of about 2000 pixels, the pixel scale due to the digitization is thus about $1''/\text{pixel}$. Information about log-book notes, plate dimensions, and contents is available on the project web-page².

The bulk of the *MW* images we analyzed are the reduced-size (800×800 pixels) science quality FITS files posted for distribution on the UCLA project web-page. The

¹ <http://cvs3.mporzio.astro.it/~cvs/cvs/arcetri.html>

² http://www.astro.ucla.edu/~ulrich/MW_SPADP/

file headers of these images contain information about the acquisition of the original plate and its digitization, as well as measurements of the disk horizontal and vertical radii. These images were also processed in order to remove small-scale plate inhomogeneities, as described in the project web-page. We analyzed 34166 images obtained on 20684 observing days.

In addition, we have also analyzed two other samples of *MW* images. The first sample contains 237 full-size images, which have thus $\approx 2600 \times 2600$ pixels each, taken in the month of July from 1920 to 1930. These images are 16-bit FITS files. The file headers of these images contain information about the radius and disk center of the solar observations. The analyzed images were also processed by the UCLA scientists to remove small-scale inhomogeneities. The analysis of this sample aims at evaluating the sensitivity of the results to the reduction of the image size. The other sample analyzed contains 713 reduced-size images (800×800 pixels) which were photographically calibrated by the UCLA project scientists. These images were obtained by applying a calibration method based on the one presented by de Vaucouleurs (1968) with some modifications. This method makes use of calibrated exposures made on the plates outside the solar disk for the data acquired since late 1961 (details available on the project web-page). This sample contains *MW* observations taken in 1967 and 1975.

Modern data - We also analyzed a sample of Ca II K spectroheliograms obtained at the Observatory of Paris-Meudon. These data (*Me*, hereafter) consist of 1044 full-disk images taken with the updated version of the instrument installed at the beginning of the 20th century (Deslandres 1891; Deslandres & D’Azambuja 1913). This is a prism-spectroheliograph with a dispersion of $0.48 \text{ mm}/\text{\AA}$ at K_{1V} and K_3 . The size of the solar disk image is $\approx 6.5 \text{ cm}$; the image scale is thus about $0.033 \text{ mm}/''$. Images are acquired with a 1300×1300 14 bit pixel CCD camera, with a pixel scale of $\approx 1.5''/\text{pixel}$. The spectral pass-band of these images is 0.15 \AA centered on the K_3 and the K_{1V} line features (J. M. Malherbe, private communication). We analyzed 903 K_3 and 141 K_{1V} images, respectively. These images were obtained on 87 observing days in the month of July from 2004 to 2006. The data analyzed are the FITS format images available through the BASS2000 archive³.

Finally, we also analyzed a sample of Ca II K full-disk images obtained with the PSPT telescope at the Rome Observatory (Ermolli, Berrilli, & Florio 2003). These data (*PSPT*, hereafter) were recorded with a telescope designed to provide high-precision photometric observations in several spectral bands (Coulter & Kuhn 1994; Ermolli et al. 1998). Briefly, images are acquired with a 2048×2048 12 bit pixel CCD camera, $2 \times$ binned, with a final pixel scale of $\approx 2''/\text{pixel}$, using an interference filter centered on the Ca II K line (393.3 nm , FWHM 0.25 nm). In particular, we analyzed 4448 images obtained on 2838 observing days from January 1998 up to December 2006. The sample of data analyzed is composed of single frame images acquired with short exposure times, as well as images obtained by co-adding 25 frames acquired with short exposure times. In general, the addition of frames, which is aimed at a reduction of the photometric measurement noise, also re-

duces the spatial resolution on images. The data analyzed are the FITS format images available through the Rome-PSPT archive⁴.

2.2. Definitions

Values for each pixel (pixel value, *PV* hereafter) of the *Ar*, *Ko*, and *MW* images were provided by the scanning devices and measure the flux of the scanner beam transmitted through the photographic plate. Note that the *MW* data available on the project web-page were reversed, in order to show bright solar features with higher pixel values. However, the pixel values of the *MW* images analyzed in this study describe the numbers provided by the scanner device. Given a proper scanner calibration, *PV* for each image pixel is a measure of the blackening degree of the photographic plate at the position corresponding to that pixel. The blackening is linked to the flux of solar radiation incident during the plate exposure by a relation which depends on many plate characteristics (Dainty & Shaw 1974). The knowledge of this relation, which is called characteristic curve, allows a calibration of the photographic blackening into intensity. Note that some of the image properties considered in this study do not depend on the photographic calibration of the original data. In particular, information on both geometrical distortions and spatial scale, can be obtained by analyzing photographically un-calibrated historic data. However, the evaluation of the photometric properties of the images, such as stray-light level and contrast, requires photographic calibration of the data. This holds also for the direct comparison between results obtained from historic and modern data.

Since only a small fraction of the historic images analyzed contains calibration exposures, we performed the photographic calibration of all these data using a method independent of calibration exposures. Namely, we have converted the image pixel value *PV* of the *Ar*, *Ko*, and *MW* images into relative calibrated intensity values according to the formula (Mickaelian et al. 2007): $I_i = (V - B)/(T_i - B)$, where I_i is the calibrated intensity (in arbitrary units) of pixel number i , V is the average of *PV* for the unexposed part of the plate, B is the average of *PV* for the darkest pixels, and T_i is the *PV* for pixel number i . The pixels of the unexposed part of the plate are identified in each image as the ones outside the solar disk with *PV* higher than the maximum *PV* of solar disk pixels. The darkest pixels in each un-calibrated image are the ones with *PV* lower than or equal to the minimum *PV* of solar disk pixels. The effects of modifying the criteria for the identification of darkest and unexposed pixels upon the contents of the analyzed data are presented in Sect. 4. Note that the application of this straightforward method for the photographic calibration of historic data is functional to our study, which takes into account only average image contents. The accuracy of the applied method is also discussed in Sect. 4.

The pixel values in the *Me* and *PSPT* images were provided by a CCD recording device. Given a proper instrumental calibration, the pixel values in both *Me* and *PSPT* images are almost linearly proportional to the flux of radiation incident during the exposure of the device.

³ <http://bass2000.obspm.fr>

⁴ <http://www.mporzio.astro.it/solare>

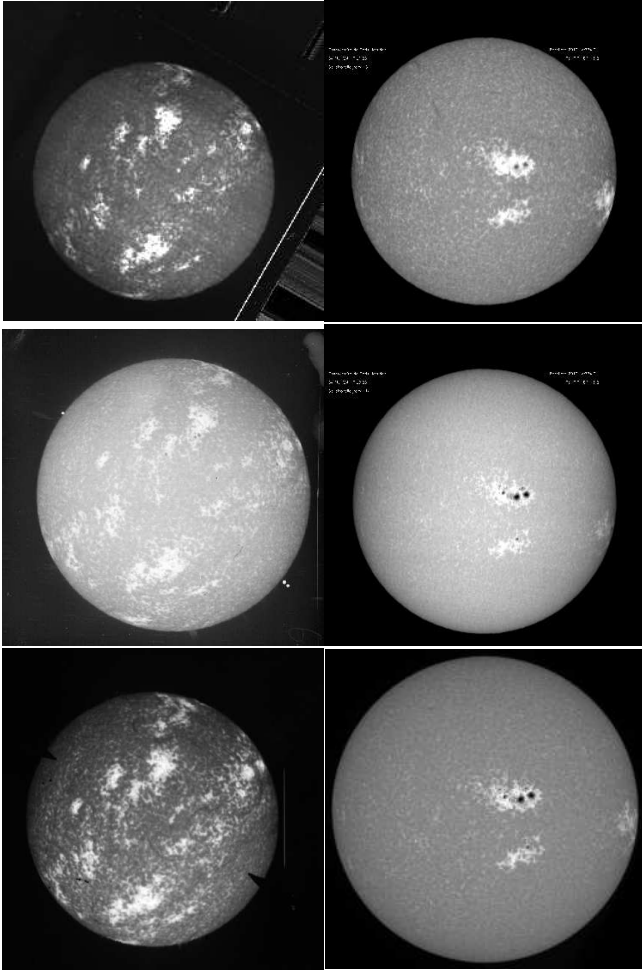


Fig. 1. Examples of the Ca II K observations analyzed in this study. Left: Arcetri (top), Kodaikanal (middle), and Mt Wilson (bottom) historic images obtained by the digitization of spectroheliograms taken at the three sites on January 9, 1958. All these images show sunspots when inspected at full resolution; the Mt Wilson image (bottom) clearly shows also on-disk filaments. The Arcetri image (top) shows signs of a filament near the right limb (in the lower activity belt). Note that the pixel values were reversed, in order to show the brightness pattern as is usually observed in the intensity images of the solar disk. Arcetri and Kodaikanal images were also rotated to liken the Mt Wilson solar observation. Right: K_3 (top) and K_{1V} (middle) Meudon spectroheliograms and Rome-*PSPT* filtergram (bottom) taken at the two sites on July 24, 2004 ($\approx 07:20$ UT).

2.3. Data inspection

The visual inspection of images shows considerable differences between the solar observations taken on the same day from the three historic series (Fig. 1). For instance, the *MW* images show filaments over the solar disk, which are not found in the other data, although some are hinted at in the *Ar* images. On the other hand, *Ko* images show sunspot regions which are almost absent in the *MW* observations, and are partly found in the *Ar* data. Moreover, the position, dimension, and number of bright features identified in the images are quite different, especially close to the solar limb. The different observing time at the three sites,

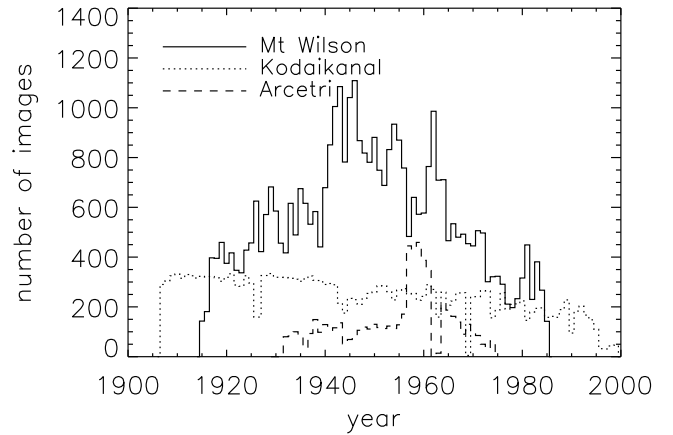


Fig. 2. Temporal coverage of the Mt Wilson (solid line), Kodaikanal (dotted line) and Arcetri (dashed line) historic time-series and the number of Ca II K images per year analyzed in this study.

which may differ by more than 16 hours due to the site location, can explain part of these differences. However, the bulk of them arise from the different spectral sampling of these observations. In particular, observations taken with a narrow spectral sampling centered at K_3 show on-disk filaments, while the ones taken in a spectral range including the $K_{1V,1R}$ show sunspots. The *Me* and *PSPT* data show all the solar features listed above. Their visual inspection also reveals small differences between the observations taken at the two sites on the same day.

The temporal coverage by the historic series and the number of images per year available for our study are shown in Fig. 2. It is seen that the *Ar* series contains a rather small number of images with respect to the other ones. However, more than 65% of the images in this series have exposure wedges for the calibration of the non-linear response of the photographic emulsion. In contrast, most of both *MW* and *Ko* images (75% and 55%, respectively) do not have wedge calibrations. The *Ar* series is thus particularly suitable for a study and comparison of different calibration methods based on either calibration exposures or other criteria, such as the use of the solar intensity limb darkening or intensity distributions. The *Ko* series covers the largest period of observations. Since not all the original plates were digitized, the full set of data stored in the Kodaikanal archive is also more extensive than suggested by Fig. 2. However, the *Ko* images were digitized with a lower bit-significance compared to the two other historic series. For instance, visual inspection of images reveals compression effects on the small scale blackening pattern, which are typically associated with lower resolution image formats. Moreover, the 8-bit dynamic range of the digitized images often compresses the actual dynamic range of the blackening distribution on the original plates, mostly when plate defects, such as emulsion holes and scratches, are present. Because of this compression, the small-scale density patterns inside both darker and brighter features on the plates are lost. Finally, the *MW* data look most promising, when taking into account both their nominally higher image quality and the large number of images available, although over a shorter length of time than the one covered by the *Ko* data.

The visual inspection of the three historic series reveals some specific defects in these data caused by instrumental

problems, as well as by the circumstances surrounding observations and storage. For instance, sometimes thick bright lines and bands in the direction of the spectrograph slits are seen in un-calibrated images. These lines and bands were likely caused either by irregularities in the drive rate for the image scanning or by shadows due to the passage of clouds or due to objects in the optical path during observations. Sometimes variations of the resolution over the solar disk within one image are observed, which are caused by changes in the atmospheric turbulence during the observation. A number of un-calibrated images show tiny bright lines across the solar disk, perpendicular to the slit. These lines were probably produced by irregularities or dust particles in the optical path of the spectroheliograph (e.g. on either entrance or exit slits). On the other hand, handling and storage of the plates for several decades have also led damages in the plate emulsion. These are seen as bright scratches and holes in un-calibrated images.

Our inspection has also revealed other frequent problems of these data. Variation of the solar declination during observation, curvature of the spectrograph slits, and small differences in the velocity setting of drive motors in the instrument resulted in geometric distortions of the solar image. In particular, the solar disk often appears elliptic, the axes of the ellipse being parallel and perpendicular to the spectrograph slit. Note that the position of these axes with respect to the horizontal and vertical directions in the analyzed images depends on the optical path of the spectroheliographs used to get the original photographic observations, as well as by the positioning of the photographic plate in the digitization device.

The historic un-calibrated data also display large-scale blackening patterns. Often they are most clearly seen outside the solar disk, but they also affect the solar images. These patterns are due to stray-light introduced by the instrument optics and by the turbulence in the Earth atmosphere. Some images show localized blackening patterns, which may be due to chemical effects during the plate development. Data inspection clearly shows also that blackening values in the historic solar images vary in a broad range. Such blackening differences are probably produced by modifications of the instrumentation and of the observational procedures, as well as of the photographic processing of the original plate. We also noticed occasional spectrally off-band observations.

Note that the defects listed above occur to different degrees in the three analyzed historic series. For instance, the *Ko* images are, on average, less affected by defects, such as scratches, lines, and geometrical distortions, than both the *Ar* and *MW* data. However, this is probably due to the fact that the *Ko* data-set contains only the highest-quality plates, selected from the Kodaikanal archive prior to digitization.

Finally, it is worth noting that the image size varies in two of the analyzed historic time-series, namely in *MW* and *Ko* sets. The size of *MW* images changes by up to about 4% over the whole series. It is typically larger for the data from October 1962 onward. This is mainly due to changes in the spectroheliograph on 8 October 1962. The new optics gave an about 1.75 times larger image of the Sun. In order to keep the size of the digitized images more or less the same, a change in the scanning resolution was applied, which reduced the difference in the image size to less than 4% but did not remedy it completely. The size of *Ko* images

for three periods, namely 1927, 1950-1955, and 1991-1999, is only half of the size of all other *Ko* data. Note that changes in the setup of the digitization device, such as the size of the digitized image, may also determine variations of the image contents. *Ko* data during these periods are not included in our analysis. This is meant to ensure that no bias due to the original different pixel sizes enters the results.

Most of the problems listed here, including variations of the image size, geometrical distortions, large scale intensity patterns and stray-light, are discussed in more detail in Sect. 3.

2.4. Image pre-processing

The analyzed images of the *Ar* and the *MW* series were independently pre-processed in order to apply the flat-field calibration of the digitization device. Details about the applied methods are given by Centrone et al. (2005) and by the UCLA project web-page for the *Ar* and *MW* series, respectively. On the other hand, visual inspection of *Ko* images shows that this series lacks such preliminary calibration. In fact, accumulation of dust and some defects in the digitization device can easily be noticed in the data. Due to the lack of information on the flat-field response of the digitization device, this pre-processing step is missing for this series. Note that the measurement of the average image contents considered in this study is only slightly affected by dust accumulation and device defects. However, these defects may lead to inaccurate determination of solar features during any subsequent image-processing. The analyzed images of the *Me* and the *PSPT* series were independently pre-processed in order to apply the flat-field calibration of the CCD recording device. Details about the applied methods are given in the pertinent references listed in Sect. 2.1.

Photographic calibration of images described in Sect. 2.2, as well as analysis of image contents described below, requires the knowledge of both, position of the center and radius of the observed solar disk. For the *MW* images, information about the solar disk center, disk horizontal and vertical radii, and the quality of their measurements is stored in the FITS headers of images. They were determined by the UCLA project scientists by applying a four-step algorithm, which was designed to be robust against a variety of image defects and of image contents. The algorithm is repeated until trial results no longer change. For properly exposed images, it is known that the algorithm tends to over-estimate the solar disk size compared with typically adopted values. Details about the algorithm can be found on the project web-page.

The headers of *Ar*, *Ko*, *Me*, and *PSPT* images do not contain information about solar disk centre and radius measurements. We determined each independently using a method consisting of three steps. It is partly based on automated techniques described in the literature (e.g. Walton et al. 1998; Denker et al. 1999; Zharkova et al. 2003). In brief, the method searches for the solar rim, by marking the location of pixels in which two selection criteria are simultaneously fulfilled. The two criteria are: 1) the value of the marked pixel is higher than a given threshold value, which is computed taking into account the mean value of pixels belonging to a sub-array centered at the baricenter of pixel values of the image; 2) the gradient of pixel values along the analyzed half-line finds a maximum

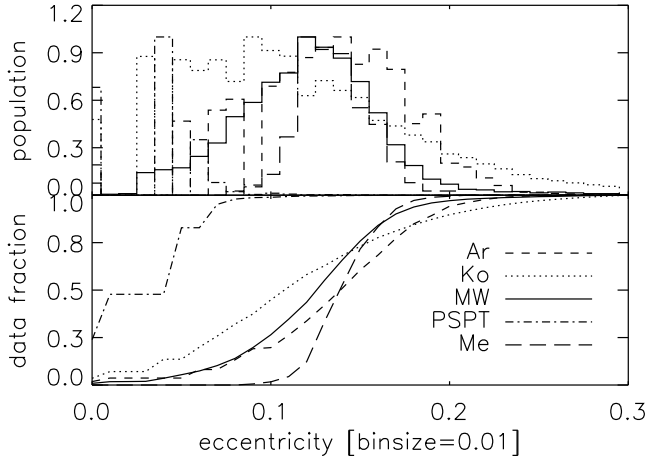


Fig. 3. Solar disk eccentricity for the analyzed data. Top: Histograms of the eccentricity values. Bottom: Cumulative histograms of the measured values. The time-series corresponding to each line style is described by the legend in the bottom panel.

value at the marked pixel. The search is performed along 360 half-lines, taking into account all pixels belonging to each analyzed half-line until the criteria are fulfilled. The half-lines originate in the baricenter of pixel values of the image. The position of the marked pixels, i.e. the solar rim is then used for the computation of the disk center and shape, which is performed by applying an ellipse-fitting algorithm. On average, this method gives values of the horizontal and vertical radii of *MW* solar observations which are about 1.5 pixel smaller than those given in the file headers. This difference corresponds to less than 0.5% of the radius. Note that each historic series analyzed in this study shows specific characteristics and artifacts such that the algorithm for centre and radius measurements needs considerable modifications for application to each series.

Most of the results presented in the following were obtained by analyzing re-sized images. This is to ensure a similar solar disk size in all series, and thus to allow their direct comparison. Moreover, this image re-sizing also helps to compensate for the geometrical distortions affecting some of the analyzed data. Both horizontal and vertical radii of the solar disk are re-sized to 350 pixels in all images, i.e. roughly to the size of the *MW* data. By this image re-sizing, the *Ar* and *Ko* data are re-sampled to about half the linear size of the original digital images. For comparison, results obtained by the analysis of full-size data are also presented below.

3. Data contents

We measured several quantities in each image of the analyzed series in order to evaluate the data contents and the homogeneity in time of such data. Measurements for historic data were performed on photographically calibrated images, which were obtained from the original data as described in Sect. 2.2.

3.1. Geometrical distortions

The main geometrical distortions affecting the analyzed data are revealed by the parameters of the ellipse which

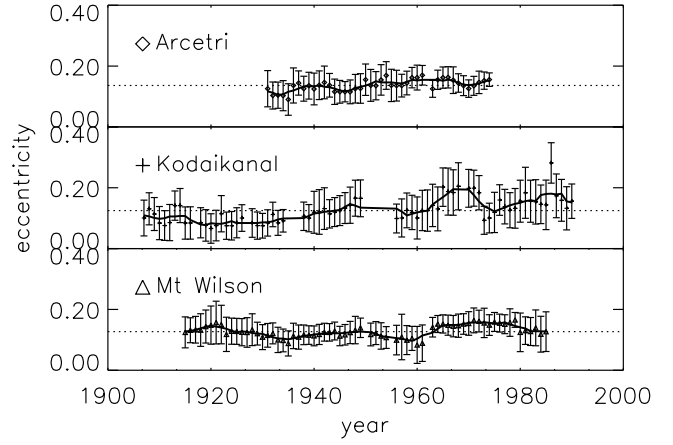


Fig. 4. Temporal variation of the solar disk eccentricity for the *Ar*, *Ko*, and *MW* series. The error bars represent the dispersion of measurements in terms of their standard deviation. The dotted line marks the median value of the average annual results for the whole series. The solid lines represent 5-year running means.

best fits the solar disk edge. We found that the difference between the major and minor axes of the ellipse for the *Ar*, *Ko*, and *MW* series is, on average, $\approx 2\%$, $\leq 1\%$, and $\leq 1\%$ of their mean value, respectively. The analysis shows that *Ar* and *MW* series suffer from geometrical distortions, which are predominantly in the horizontal and vertical directions. In contrast, the orientation of the best-fit major and minor axes of the ellipse to *Ko* images rotates depending on the observation time. In order to compare homogeneous quantities for the data-sets, hereafter we take into account the ratio between the horizontal r_x and vertical r_y radii in each solar image. We also compute the solar disk eccentricity $e = \sqrt{1 - (r_{min}/r_{max})^2}$, where r_{min} , r_{max} are the smallest and the largest radii of the solar image in the horizontal and vertical directions.

We found that the average value and the standard deviation of the disk eccentricity for the *Ar*, *Ko*, and *MW* images are 0.14 ± 0.04 , 0.12 ± 0.06 , and 0.12 ± 0.04 , respectively (Fig. 3). The same measurements carried out on *Me* and *PSPT* images give 0.14 ± 0.02 and 0.04 ± 0.03 , respectively. We thus found that disk eccentricity of both historic (*Ar*, *Ko*, and *MW*) and modern (*Me*) spectroheliogram observations is about 3 times larger than the one computed for modern observations taken with interference filters (*PSPT*).

The standard deviation of annual averages of the disk eccentricity for the *Ar*, *Ko*, and *MW* time-series is ≈ 0.02 , 0.04 , 0.02 , respectively, i.e. about 14%, 32%, 15% of the median values (Fig. 4). However, the standard deviation of the values measured over a year, due to, for example, seasonal variations and occasional failures of the algorithms used for radii measurements, is on average about twice as large as the variation of the values on longer time-scales. Note the slight continuous increase of disk eccentricity in the *Ar* series and the marked increase of the dispersion of results obtained for the *Ko* data taken from about 1960 onward. This latter effect is mostly due to a marked decrease of the image quality and a subsequent increase of failures in the ellipse fitting calculations. In contrast, the geometrical distortion of solar disk observations on *MW* data remains

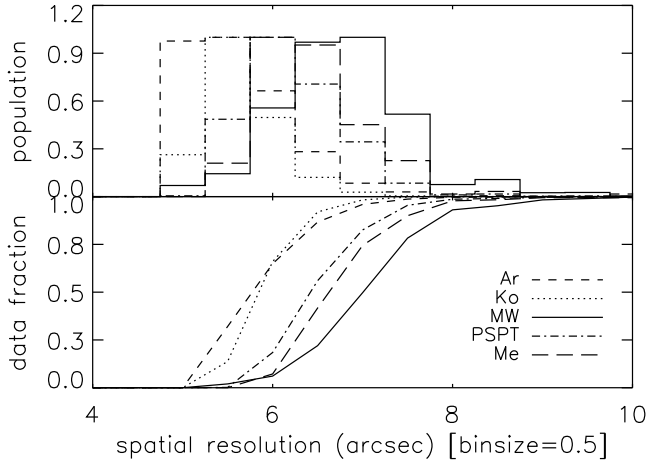


Fig. 5. A measure of the spatial resolution of the analyzed data. Details are given in Sect. 3.2. Legend as in Fig. 3.

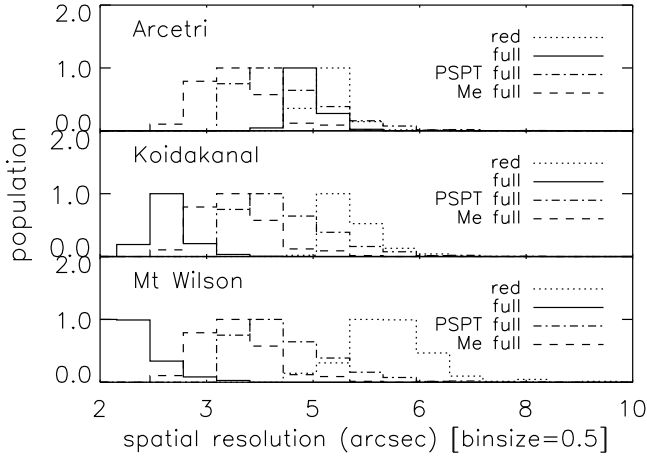


Fig. 6. Histograms of the spatial resolution measured on both full-size (solid line) and reduced-size (dotted line) images corresponding to the same sample of original historic observations. The dashed and dot-dashed histograms show the results obtained for the full-size *Me* and *PSPT* data, respectively.

almost constant over the whole series. The measured value slightly increases for the data taken from 1962 onward.

3.2. Spatial resolution

In order to evaluate the spatial resolution of each analyzed image, we studied the power-spectra of a 64×64 sub-array extracted at solar disk center. In particular, we measured for each image the spatial frequency at which 98% of the image power spectral density is taken into account. The bulk of the information about patterns in the images lies at frequencies below this. The spatial scale corresponding to this measured cut-off frequency is taken as a measure of the spatial resolution in the analyzed image. Note that the power density never decreases below a noise level for some data due to image defects. This is the reason we did not employ the usual technique of noting the spatial frequency at which the power drops to the noise level. The usage of a small sub-array and of the 98% threshold is aimed to avoid

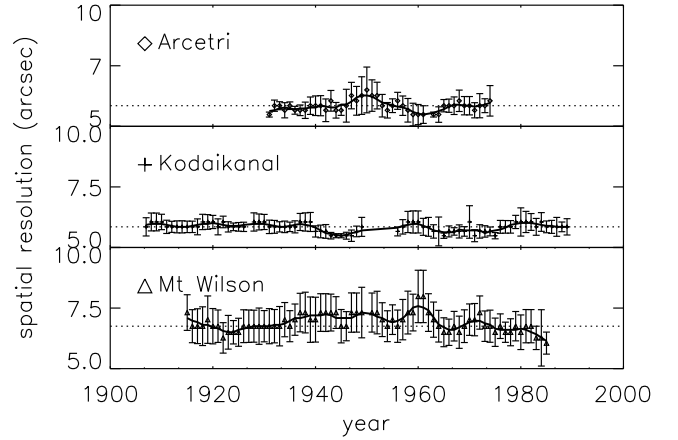


Fig. 7. Temporal variation of the spatial resolution evaluated on the *Ar*, *Ko*, and *MW* images. Legend as in Fig. 4.

the detection of power associated with the occurrence of solar features and image defects, respectively.

The average spatial resolution and its standard deviation on *Ar*, *Ko*, and *MW* images are $5.9 \pm 0.2''$, $5.9 \pm 0.1''$, and $6.9 \pm 0.6''$, respectively, when considering images re-sized to the same solar disk size (Fig. 5). Thus, on average, *Ar* and *Ko* images appear to carry more spatial information than the *MW* data, although the difference is rather small. On the other hand, the average spatial resolution of *MW* images is close to the ones of current *Me* and *PSPT* observations, which are $6.6 \pm 0.4''$ and $6.5 \pm 0.3''$, respectively. These results can be partly explained by the differences in the spectral sampling of the analyzed series. In fact, the nominal narrower spectral sampling of *MW* data with respect to the other historic series, corresponds to observations of higher atmospheric levels compared to the others, and thus to observed features characterized by lower spatial details. This holds also for *Me* images.

The average spatial resolution computed for the historic data is close to the one associated with the Nyquist frequency of the analyzed reduced-size images. In order to evaluate whether the image re-sizing leads to a loss of spatial resolution stored in the original data, we analyzed samples of *Ar*, *Ko*, and *MW* full-size images. We found that the average spatial resolution and its standard deviation in the sample of full-size *MW* images are $2.6 \pm 0.2''$, compared to $6.6 \pm 0.5''$ obtained for the same sample of observations with the reduced-size images (Fig. 6). These values for *Ko* full-size data are $3.3 \pm 0.1''$, compared to $6.04 \pm 0.13''$, for the same sample of observations with the reduced-size images. Finally, the values obtained for *Ar* full-size data are $5.4 \pm 0.1''$, compared to $5.74 \pm 0.06''$, for the same sample of observations with the reduced-size images. For comparison, the same quantities evaluated in the samples of full-size *Me* and *PSPT* images are $5.0 \pm 5.0''$ and $5.0 \pm 0.4''$, respectively.

The average spatial resolution measured on *Ar*, *Ko*, and *MW* full-size images is also close to the one limited by the spatial sampling of the analyzed data. Moreover, we found that the values of the average resolution measured at the solar disk centre and outside the solar disk are within one standard deviation in measurements. These results suggest that the power density found at the smallest spatial scales in the full-size data depends on image digitization. We then analyzed the resolution measured at the solar disk centre on

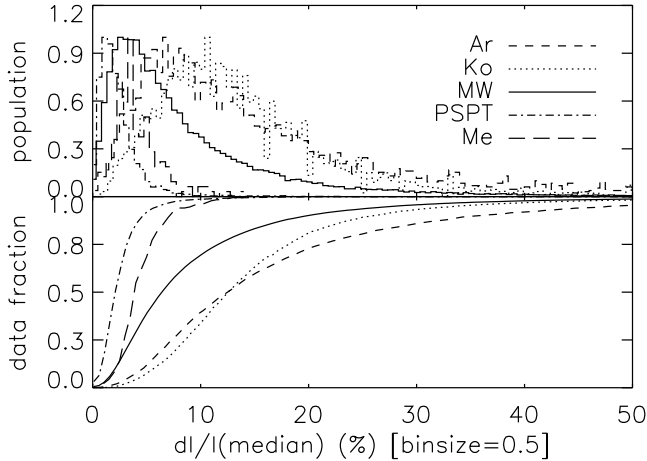


Fig. 8. A measure of the large-scale inhomogeneities affecting the analyzed data. Details are given in Sect. 3.3. Legend as in Fig. 3.

images re-sized using linear interpolation to half, one-third, and one-fourth the original dimension. We found that the resolution measured on each set of re-sized images shows a skewed distribution of values, with a longer tails to the right of the distribution maximum. We computed the moments of these distributions. The obtained values indicate that the distribution resulting from images re-sized to half the original dimension is the most symmetric about the maximum, as well as the less peaked, among the ones we studied. The obtained values also suggest that the re-sizing of images to more than half the original dimension implies a loss of spatial information for the solar observations stored in the full-size data.

The analysis of the temporal variation of the image resolution for each series allows an evaluation of the homogeneity of the data in each data-set. We found that the spatial scale of all the three historic series varies slightly in time (Fig. 7). In particular, the standard deviation of averaged annual values for the *Ar*, *Ko*, and *MW* series is about 4%, 3%, 5%, respectively. However, the standard deviation of values measured over a year is on average about twice larger, due to seasonal variations of the image contents.

Figure 7 shows that the spatial resolution on the *MW* images has steadily increased in the last two decades of observations. This variation is likely due to instrumental changes (e.g. differences in the spectral sampling of the data). Note that the variation of image size affecting the *MW* data also contributes to the increase of the spatial resolution measured for *MW* images from 1960 onward. However, the measured resolution increase is about 20% larger than the one expected by taking into account the variation of the solar disk size in the analyzed images. Finally, our results suggest that the spatial resolution of the *Ko* data remains almost constant over the whole period.

3.3. Large-scale image inhomogeneities

Next we considered some photometric properties of the analyzed series. We first evaluated the level of large-scale inhomogeneities in the images introduced by variations of the sky transparency during observations and by instrumental problems. In particular, we analyzed the median intensity

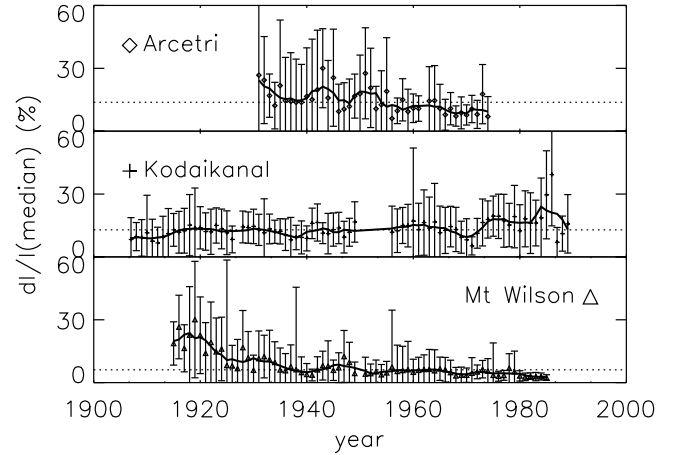


Fig. 9. Temporal variation of the results obtained measuring the large-scale inhomogeneities affecting the *Ar*, *Ko*, and *MW* images. Legend as in Fig. 4.

over a ring centered on the solar disk center of each image. The ring spans the disk positions $\mu=0.50\pm0.05$. Since strong inhomogeneities may affect only a portion of the solar image, we divided the solar disk into four quadrants and calculated the deviation of the median intensity value in each quadrant, with respect to the median value over the whole ring. We then took the maximum deviation measured over the four quadrants as a measure of the degree of large-scale intensity inhomogeneities affecting the solar disk images. Note that usage of median intensity values and of the disk positions $\mu=0.50\pm0.05$ is aimed to lower the influence of active regions on the obtained results.

We found that the median value and the standard deviation of measurements for the *Ar*, *Ko*, and *MW* series are $13\pm17\%$, $12\pm6\%$, and $6\pm6\%$, respectively (Fig. 8). The same quantities evaluated for the *Me* and *PSPT* data are $3.9\pm2.2\%$ and $2.2\pm2.2\%$, respectively. The standard deviation of measurements for each series is about 43%, 37%, and 96%, which is close to the average of the standard deviation of values measured over a year for the *Ar* and *MW* series, and half the one for the *Ko* series.

We found that the first half of the *Ar* series, as well *MW* data taken during the first decade of observation suffer from strong large-scale inhomogeneities (Fig. 9). This is in agreement with information stored in *MW* log-book notes which report that image vignetting was very strong at that time due to the use of an under-sized grating.

3.4. Stray-light

We evaluated the level of stray-light in the data by checking the fall-off of intensity values just outside the solar limb (aureola, hereafter) in each image. For this, we computed the median intensity over rings centered on $\mu = 1$ and evaluated the profile of these median values in each image, starting from the disk centre up to the image edge. Each ring is one pixel thick. In order to compare the stray-light level in all series, we have then used these calculated radial profiles to evaluate the ratio of the intensity values at fixed off-limb distances (e.g., $r/R_{sun}=1.06\pm0.01$, 1.125 ± 0.025 , 1.225 ± 0.025) to that at the disk center ($I/I(0)$, hereafter). Note that analysis of aureola regions close to the solar disk ($r/R_{sun} < 1.3$) is aimed to avoid the influence of strong in-

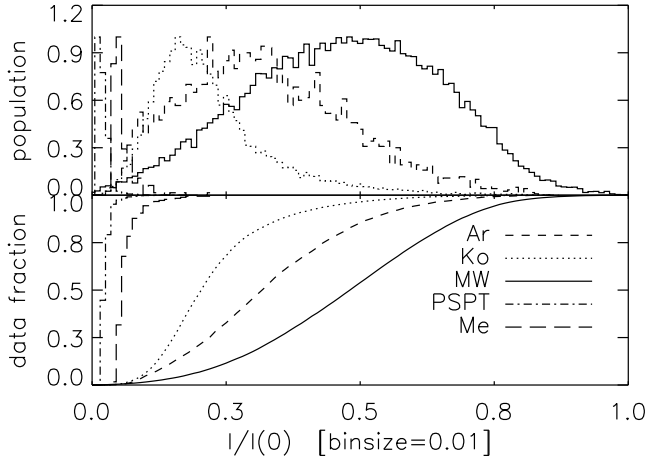


Fig. 10. A measure of stray-light level on the analyzed data. These results concern aureola measurements at $r/R_{Sun} = 1.06 \pm 0.01$. Details are given in Sect. 3.4. Legend as in Fig. 3.

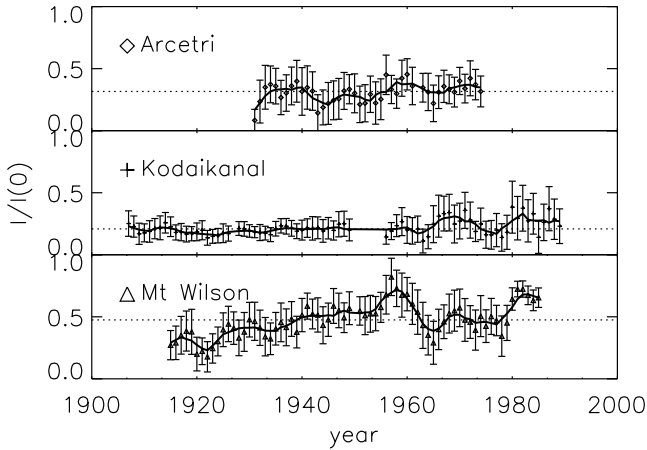


Fig. 11. Temporal variation of stray-light level on the *Ar*, *Ko*, and *MW* images. Legend as in Fig. 4.

tensity inhomogeneities often observed outside of the solar disk. These inhomogeneities are mostly due to unexposed plate regions, calibration exposures, and inscriptions on the original plate. Figure 10 compares the results of our estimates of the stray-light at $r/R_{sun}=1.06 \pm 0.01$ for all datasets calibrated as described in Sect. 2.2. The dependence of the obtained results on the calibration method applied to the original data is presented in Sect. 4.

We found that historic *Ar*, *Ko*, and *MW* images are strongly affected by stray-light, much more than modern *Me* and *PSPT* data. Moreover, *Me* spectroheliograms suffer more from stray-light than *PSPT* filtergrams. The median value and the standard deviation of the measured intensity ratio at $r/R_{sun}=1.06 \pm 0.01$ for *Ar*, *Ko*, and *MW* images are 0.32 ± 0.15 , 0.20 ± 0.11 , and 0.48 ± 0.18 , respectively. The same quantities for *Me* and *PSPT* observations are 0.05 ± 0.03 and 0.02 ± 0.01 , respectively.

The temporal variation of the stray-light level is sensitive to changes in instrumental conditions and setups. For instance, Fig. 11 shows a large reduction of the stray-light level for the *MW* data taken from 1960 onward, probably due to the installation of new gratings, which is also recorded in the observatory log-books. The results also

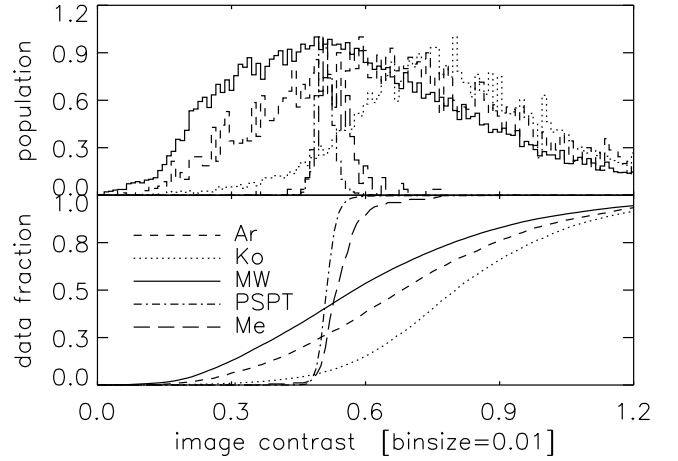


Fig. 12. A measure of the image contrast for the analyzed data. Details are given in Sect. 3.5. Legend as in Fig. 3.

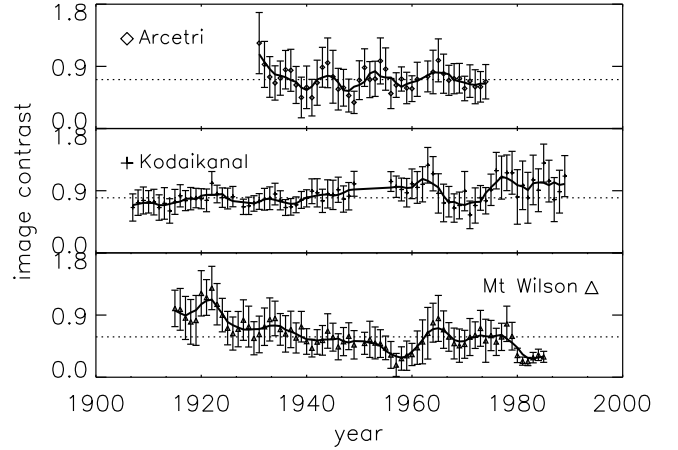


Fig. 13. Temporal variation of the image contrast on the *Ar*, *Ko*, and *MW* images. Legend as in Fig. 4.

clearly show effects of the aging of both instruments and observing programs. In fact, the stray-light level increased with grating use, since that component degraded in the open air installation of the spectrograph. The standard deviation of annual averages over the *Ar*, *Ko*, and *MW* series is about 25%, 29%, and 28%, respectively. The standard deviation of values measured over a year due to seasonal variations of the image quality is about 8, 1.3, and 1 times larger for the three series, respectively.

3.5. Image contrast

Next we considered the range of intensities measured in the solar images of each time-series. In particular, we analyzed the center-to-limb variation of intensity values of quiet Sun regions (*CLV*, hereafter) and measured the maximum minus the minimum intensity values, normalized to their mean (henceforth, image contrast). The *CLV* was evaluated on each image by computing the median of intensity values over each of 20 rings of equal area centered on the solar disk center. Maximum and minimum intensity values are the largest and the smallest values among the 20 intensity values thus determined. Note that usage of the small number of rings and of the median intensity in each ring is

aimed to lower the influence of image defects and of active regions on the obtained results.

The median value and the standard deviation of the image contrast for *Ar*, *Ko*, and *MW* images are 0.7 ± 0.3 , 0.8 ± 0.2 , and 0.6 ± 0.3 , respectively (Fig. 12). The same quantities for *Me* and *PSPT* images are 0.53 ± 0.05 and 0.51 ± 0.04 , respectively. Note that the standard deviation of contrast measurements for modern data is about 10 times lower than that for historic data. This may partly be due to the larger samples of images covering longer periods of time compared to the modern sets. However, the main reason is probably the higher degradation due to stray-light and the uncertainties in the photographic calibration of the historic data. For instance, the method applied in this study to perform the photographic calibration makes use of pixel values of both unexposed and dark regions of the original plate, which might be badly defined in the analyzed data. Note that the median value and the standard deviation of measured image contrasts for the three historic series are very similar. Thus the results obtained are not affected by differences in the solar disk center determination and shape calculations performed on the three series.

Figure 13 shows the temporal variation of image contrast for the three historic time-series. Changes in instrumentation and the observing procedure are well seen. The annual averages of the image contrast is found to vary by about 0.17, 0.16, and 0.23, i.e. by about 23%, 20%, and 40% of the median values for the *Ar*, *Ko*, and *MW* series, respectively. The standard deviation of values measured over a year, which takes into account seasonal variations of the image quality, instrumental changes, and occasional failures of the algorithms used for radii measurements, is close to the standard deviation of the annual averages.

4. Discussion

We have analyzed the image contents of three historic time-series of Ca II K observations obtained by the digitization of photographic archives of Arcetri, Kodaikanal, and Mt Wilson spectroheliograms. The results have been compared to those obtained for the modern synoptic Ca II K observations taken with the Meudon spectroheliograph and the Rome-PSPT telescope. We have also analyzed the temporal variation of the image contents, in order to evaluate the homogeneity of the three historic time-series.

This study shows that historic spectroheliograms suffer from stronger geometrical degradation and large-scale inhomogeneities than modern filtergrams, but at a similar level to present-day spectroheliograms. Historic data also suffer from stronger pixel-scale image defects than current observations. Some of these defects are accountable to the aging of the original observations, some are due to shortcomings of the instruments. They can partly be corrected for or taken into account by a proper analysis. We find these issues bothersome, but not as serious as problems related to the photometric properties of the historic spectroheliograms. In particular, both the average value and the standard deviation of the stray-light level are higher in the historic data than in the modern ones. This holds also for the image contrast. The difference in the image contrast is particularly worrisome since this lies at the heart of the scientific evaluation of the historic images. It may be caused by differences in spectral sampling (e.g. if historic and mod-

ern data were to sample different parts of the line profile), calibration issues, or degradations due to stray-light.

Peculiarities in the spectral sampling of the historic data seem unlikely to be responsible for the differences in image contrast described above. In fact, we measured the relative difference between the *CLV* curves computed for *K₃* and *K_{1V}* *Me* images recorded on average less than 2 minutes apart. We found that the dispersion of the *CLV* curves computed for the *Me* images obtained with the two spectral samplings in the same observing day is smaller than the dispersion of results obtained for spectrally homogeneous data taken on different days. In particular, the median value and the standard deviation of the relative difference between the *CLV* curves computed for the two samples of spectral images are -0.006 ± 0.016 for all disk positions $\mu \geq 0.4$. The same quantities computed for the sample of *K₃* images, with respect to a randomly selected *K₃* image are -0.003 ± 0.020 . This result is in agreement with the findings of a similar analysis which we performed on a few Ca II K spectroheliograms taken recently at the Coimbra Observatory⁵.

In order to evaluate the effects of the photographic calibration on the results presented above, we analyzed images obtained by applying three different calibration methods to the same sample of 713 *MW* observations. The three methods are: 1) the one applied by the UCLA project scientists (*UCLA*, hereafter), which takes into account the calibrated exposures available on the side of the solar observations; 2) the method described in Sect. 2.2 (*calib*, hereafter); 3) the method which assumes a linear relation between the pixel values in the analyzed images and the incident flux (*linear*, hereafter). It is worth noting that after the conversion of the plate blackening to intensity through the use of the step-wedge exposure, the *MW* images were further adjusted by the UCLA project scientists for the effect of a variable vignetting function, which yield large-scale intensity patterns in the observations not associated with the solar limb-darkening variation of intensity. The vignetting function was derived by the UCLA project scientists under the assumption that the limb-darkening variation of intensity computed on calibrated images matches some modern measurements (Livingston & Sheeley 2008). After this adjustment, the *CLV* evaluated on each *MW* image depends on both the photographic calibration applied to original images and on the removal of vignetting effects on images. Therefore the value of photometric measurements performed on the data relies on the precision of both image processing steps.

We found that the range of intensity values for quiet Sun regions obtained from the *UCLA* calibrated sample is smaller than that computed for the other two samples of images for all disk positions $\mu > 0.25$, which corresponds to about 95% of the solar disk. The dispersion of *CLV* curves over 90% of the solar disk is about 25%, 33%, and 76% for the *linear*, *calib*, and *UCLA* image samples, respectively. In summary, the intensity *CLV* of quiet Sun regions computed for the *UCLA* calibrated sample is flatter than the ones obtained with the other two samples of data, but the dispersion of curves computed from one day to the next

⁵ This set of observations is composed of images obtained for different spectral sampling by the instrument, both the spectral position and the bandwidth along the Ca II K line. The images were kindly provided by A. Garcia (Coimbra Observatory).

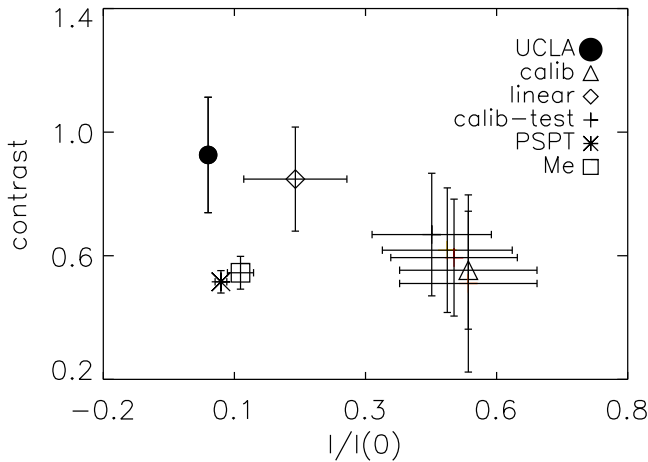


Fig. 14. Scatter plot between the mean values of image contrast (ordinate, contrast) and stray-light measurements (abscissa, $I/I(0)$) obtained for *MW* historic observations taken in 1967 and photographically calibrated with three different methods (*UCLA*, *calib*, and *linear*). Results obtained by applying the *calib* method through different numerical criteria are also shown (*calib-test*). Details are given in Sect. 4. For comparison, the same quantities evaluated for modern *Me* and *PSPT* data are also plotted. Error bars represent the standard deviation of measurement results.

for the *UCLA* sample is larger than the ones for the other samples.

Figure 14 shows the relation between image contrast and aureola intensity measurements for the three data-sets of images obtained by applying the *UCLA*, *calib*, and *linear* calibration methods to the same set of *MW* observations. For comparison, results obtained for modern data are also shown. We found that the mean value of the image contrast measured on *MW* images varies up to about 25% depending on the calibration method applied to the data. Figure 14 shows also the results obtained by applying the *calib* method with different numerical criteria for the identification of the unexposed and the darkest pixels of the images. In particular, the pixel identification was performed by using four sets of threshold values, which are based on: 1) maximum and minimum values of *PV* measured inside the solar disk; 2) maximum and minimum values of *PV* measured on the whole image; 3) higher than $m + 3\sigma$ and lower than $m - 3\sigma$, where m and σ are the mean and the standard deviation of *PV* measured inside the solar disk, respectively; 4) constant values (32767 and 0, respectively). The results obtained (*calib-test*, hereafter) are shown in Fig. 14, represented by crosses. We found that the image contrast measured on the analyzed data changes by about 10% by modifying the numerical criteria as described above.

Note that the values measured on both *calib* and *calib-test* images approaches the ones resulted for modern observations (*Me* and *PSPT*). However, the standard deviation of the values measured for both *calib* and *calib-test* historic images is about 4 times larger than the ones resulting for modern observations.

5. Conclusions

We have analyzed the image contents of three historic time-series of Ca II K spectroheliograms obtained by the digi-

tization of the Arcetri, Kodaikanal, and Mt Wilson photographic archives. Perhaps unsurprisingly, our study shows that historic data suffer from stronger degradation effects associated with instrumental problems than similar modern observations. Some of the image problems described in this study, e.g. geometrical and image defects, can be fixed through the development and application of a proper image processing technique, as we have shown. For instance, the solar disk ellipticity can be compensated by re-sizing the analyzed images. Some other problems, such as the degradation of the spatial resolution within one image due, for example, to instrumental problems, can only partly be solved through the application of sophisticated image processing. Historic data also suffer from strong photometric uncertainties due to often missing or poor photographic calibration. In addition, stray-light effects are much stronger in historic data than in modern observations. Therefore a special analysis is needed in order to check whether and to what extent the methods presented in the literature for the photometric calibration of data can restore the historic Ca II K images to a homogeneous data-set with trustable intensities. The discussion of methods for the photographic calibration and the stray-light correction of these images will be addressed in future papers.

Our results also show that the image contents of the three considered historic data-sets vary in time. These variations are, to a large extent, due to changes in and aging of the instrumentation and evolution of the observing programs. The effects of the multiple instrumental changes over many decades are even more difficult to account for with image processing than the image defects mentioned above. The temporal variations of the image contents due to instrumental changes can be singled out from solar temporal variations only through the inter-calibration of the data coming from different archives. Our results suggest that for such inter-calibration it would be extremely useful to digitize the *Ko* series with a higher quality than available at present, since the *Ko* series turns out to be the most homogeneous and longest among those considered.

This study also shows that the reliability of photometric measurements performed on historic data relies on the precision of their photographic calibration and on the removal of stray-light effects. The main challenge for the analysis of such data is thus their accurate photometric calibration, for them to provide value for studies concerning long-term solar activity and variability.

Acknowledgements. The authors thank the Arcetri, Kodaikanal, Meudon, Mt Wilson and the Rome Solar Groups for the data provided. J. Aboudarham, F. Cavallini and J.M. Malherbe are acknowledged for useful discussions. This work was partly supported by the CVS project (Regione Lazio) and by the Deutsche Forschungsgemeinschaft, DFG project SO-711/1-2. The digitization of the Mt Wilson Photographic Archive has been supported by the US National Science Foundation grant ATM/ST 0236682.

References

- Bappu, M. K. V. 1967, *Sol. Phys.*, 1, 151
- Centrone, M., Ermolli, I., & Giorgi, F. 2005, *Mem. SAI*, 76, 941
- Chapman, G. A., Cookson, A. M., Dobias, J. J., Preminger, D. G., & Walton, S. R. 2004, *Advances in Space Research*, 34, 262
- Coulter, R. L. & Kuhn, J. F. 1994, "Solar active region evolution: comparing models with observations", Balasubramaniam, K. S. & Simon, G. W., eds., *ASP Conf. Ser.*, 68, 37
- Dainty, J. C. & Shaw, R. 1974, *Image Science*, Academic (Press)

- Denker, C., Johannesson, A., Marquette, W., Goode, P. R., Wang, H., & Zirin, H. 1999, *Sol. Phys.*, 184, 87
- Deslandres, H. 1891, *Comptes Rendus Acad. Sci. Paris*, 131, 307
- Deslandres, H. & D’Azambuja, L. 1913, *Comptes Rendus Acad. Sci. Paris*, 157, 413
- de Vaucouleurs, G. 1968, *Applied Optics*, 7, 1513
- Ellerman, F. 1968, *PASP*, 31, 16
- Ermolli, I., M. Fofi, Bernacchia, C., Berrilli, F., Caccin, B., Egidi, A., & Florio, A. 1998, *Sol. Phys.*, 177, 1
- Ermolli, I., Berrilli, F., & Florio, A. 2003, *A&A*, 412, 857
- Ermolli, I., Tlatov, A. G., Solanki, S. K., Krivova, N. A., & Singh, J. 2007, "The Physics of Chromospheric Plasmas", Heinzel, P., Dorotovic, I. & Rutten R.J., eds., *ASP Conf. Series*, 368, 533
- Evershed, W. 1911, *MNRAS*, 71, 719
- Fuller, N., Aboudarham, J., & Bentley, R.D. 2005, *Sol. Phys.*, 227, 61
- Gasperini, A., Mazzoni, M., & Righini, A. 2004, *Giornale di Astronomia*, 3, 23
- Giorgi, F., Ermolli, I., Centrone, M., & Marchei, E. 2005, *Mem. SAIIt.*, 76, 977
- Godoli, G. & Righini, A. 1950, *Mem. SAIIt.*, 21, 4
- Keller, C.U., Harvey, J.W., & The Solis Team 2003, "Solar Polarization", Trujillo-Bueno J. & Sanchez Almeida J., eds., *ASP Conf. Series*, 307, 13
- Lefebvre, S., Ulrich, R. K., Webster, L. S., Varadi, F., Javaraiah, J., Bertello, L., Werden, L., Boyden, J. E., & Gilman, P. 2005, *Mem. SAIIt.*, 76, 862
- Livingston, W. & Sheeley, N. R. 2008, *ApJ*, 672, 1228
- Makarov, V. I., Tlatov, A. G., Singh, J., & Gupta, S. S. 2004, "Multi-Wavelength Investigations of Solar Activity", Stepanov, A. V., Benevolenskaya, E. E., & Kosovichev, A. G., eds., *IAU Symp.* 223, 125
- Marchei, E., Ermolli, I., Centrone, M., Giorgi, F., & Perna, C. 2006, *Mem. SAIIt. S.*, 9, 51
- Mickaelian, A. M., Nesci, R., Rossi, C., Weedman, D. et al. 2007, *A&A*, 464, 1177
- Mouradian, Z. & Garcia, A. 2007, "The Physics of Chromospheric Plasmas", 368, 3, Heinzel, P., Dorotovic, I. & Rutten R.J., eds., *ASP Conf. Series*, 368, 3
- Ortiz, A. & Rast, M. P. 2005, *Mem. SAIIt.* 76, 4, 1018
- Scherrer, P. H., Bogart, R. S., Bush, R. I. et al. 1995, *Sol. Phys.*, 162, 129
- Schrijver, C. J., Cté, J., Zwaan, C., & Saar, S. H. 1989, *ApJ*, 337, 964
- Skumanich, A., Smythe, C., & Frazier, E. N. 1975, *ApJ*, 200, 747
- Ulrich, R. K., Webster, L. S., Varadi, F., Javaraiah, J., Lefebvre, S., & Gilman, P. 2004, *AGU Fall Meeting Abstracts*, A3
- Walton, S. R., Chapman, G. A., Cookson, A. M., Dobias, J. J., & Preminger, D. G. 1998, *Sol. Phys.*, 179, 31
- Zharkova, V. V., Ipson, S. S., Zharkov, S. I., Benkhalil, A. K., Aboudarham, J., & Bentley, R. D. 2003, *Sol. Phys.*, 214, 89